We are IntechOpen,
the world's leading publisher of
Open Access books
Built by scientists, for scientists

4,800
Open access books available

122,000
International authors and editors

135M
Downloads

Our authors are among the

154
Countries delivered to

TOP 1%
most cited scientists

12.2%
Contributors from top 500 universities

BOOK CITATION INDEX
CLARIVATE ANALYTICS
INDEXED

WEB OF SCIENCE™

Selection of our books indexed in the Book Citation Index
in Web of Science™ Core Collection (BKCI)

Interested in publishing with us?
Contact book.department@intechopen.com

Latent Heat Thermal Energy Storage System

Ponnuraj Stella Jesumathy

Additional information is available at the end of the chapter

http://dx.doi.org/10.5772/intechopen.77177

Abstract

Latent heat thermal energy storage systems (LHTESS) are versatile due to their heat source at constant temperature and heat recovery with small temperature drop. In this context, latent heat thermal energy storage system employing phase change material (PCM) is the attractive one due to high-energy storage density with smaller temperature difference between storing and releasing functions. PCMs are generally possessed with low thermal conductivity, which leads to decreased rates of heat storage and extraction during melting and crystallization process. However, the low thermal conductivity of paraffin limits its use as a thermal energy storage material. In this chapter, experiments are conducted to investigate the enhancement of thermal conductivity of paraffin wax by adding alumina nanoparticles. Stable composites containing 5 and 10 vol% nanoparticles in paraffin were prepared by intense sonification. The thermophysical properties of the alumina nanoparticle enhanced paraffin (ANEP) specifically the melting and freezing temperature, latent heat, thermal conductivity, and dynamic viscosity were measured and compared with paraffin wax. These results as well as the thermal conductivity and dynamic viscosity variations with respect to temperature and nanoparticle volume concentration are discussed. Comparison of predicted Maxwell's model of a recent study shows higher enhancement than the Arasu predicted Maxwell's model.

Keywords: melting, solidification, latent heat, thermal conductivity, nanoparticle, phase change material

1. Introduction

Thermal energy storage technology has been garnering tremendous attention during the past two decades. In general, the thermal energy storage techniques exploit latent heat, sensible heat, and thermo-chemical. Among the aforementioned three types, latent heat thermal energy storage which employs phase change material is praiseworthy owing to its advantageous

characteristics, such as high storage density and nearly isothermal operating characteristics during the phase change process [1–5]. Consequently, it owns versatile applications in the fields of solar energy utilization, waste heat recovery, and active and passive cooling of electronic devices. Among the investigated PCMs, paraffin wax is regarded as the most promising phase change material because of its desirable characteristics such as large latent heat, minimal volume change, chemical stability, no phase segregation, nontoxicity, and commercial availability at low cost [6]. Inspite of these desirable properties of paraffin wax, the low thermal conductivity (0.21–0.24 W/m K) is its major drawback. Different approaches have been used to enhance the thermal conductivity of PCM, such as dispersion of high thermal conductive materials into PCMs, encasing the PCM within finned tubes, and impregnation of porous materials like carbon and metal foams [7]. Dispersing nanoparticles in paraffin has the potential to improve the thermal conductivity, thereby significantly improving its thermal energy storage characteristics. Zeng et al. [8] investigated the effect of copper nano wires (Cu NWs) dispersed in tetradecanol (TD). The thermal conductivity of the composite PCMs improved nine times better than that of pure PCM, when the composite PCM was containing 11.9 vol% Cu NWs. In this chapter, emulsion of alumina nanoparticles into melting paraffin wax in different volume fractions was prepared to study the thermophysical properties like melting/freezing point, latent heat, thermal conductivity, and dynamic viscosity. Stable composites were prepared, and a significant thermal conductivity enhancement is reported in this chapter. The distinguishing feature of this chapter is to compare the present thermal conductivity results of various volume fractions with the predicted Maxwell model as reported in the literature [9].

2. Preparation of nanocomposite PCMs

In the present study, paraffin wax (T_m = 58–60°C) is employed as PCM owing to its desirable properties like chemical stability, nontoxic, high latent heat capacity, etc. Al_2O_3 nanoparticles were purchased from Royal Scientific Suppliers Co. Ltd. The purity of the Al_2O_3 is 99.5%, and the particle size lies in the range of 20–50 nm. **Table 1** depicts the physical properties of paraffin wax, alumina nanoparticle [10], and nanocomposite PCM.

Nanocomposite PCMs were prepared by adding different volume fractions of Al_2O_3 nanoparticles into paraffin wax; however, no surfactant was used. **Figure 1** illustrates the steps involved in the preparation of composite PCMs with the addition of alumina nanoparticle in volume fractions of 5 and 10%. Initially, paraffin wax was heated to a temperature of 80°C, and the Al_2O_3 nanoparticles were then dispersed into the liquid paraffin wax. Suspensions were prepared by strong shear mixing at 1000 rpm for 20 min using a magnetic stirrer. The mixture was sonicated using an ultrasonic vibrator (Toshiba, India), generating ultrasonic pulses of 100 W at 36 ± 3 kHz. However, to ensure stability and homogeneity, intense sonication was done for a period of 6 hours. The mixture was kept in the liquid state throughout the process by maintaining a constant temperature of 65°C. There was no settling observed thereafter, and thus, the prepared composites were stable.

Parameter	Alumina nanoparticles	Paraffin wax, $\phi = 0$	Nanocomposite, $\phi = 10$ vol%
Latent heat of fusion, λ		121.9 J/g*	119.9 J/g*
Melting Temperature, $_{Tm}$		58.9°C*	58.6°C*
Solid density, ρ	3600 kg/m³	860 kg/m³	930.692 kg/m³
Liquid density, ρ	—	780 kg/m³	
Thermal conductivity, k	40 W/m K	0.24 (s) W/m K 0.15 (l) W/m K	0.42 W/mK @ 59°C
Specific heat, C_p	765 J/kg K	2.9 kJ/kg K (s) 2.1 kJ/kg K (l)	2686 J/kg K
Dynamic Viscosity, μ	—	0.205 Ns/m²	0.2188 Ns/m²

*Measured values (DSC)

Table 1. Physical properties of paraffin, alumina nanoparticles, and nanocomposite.
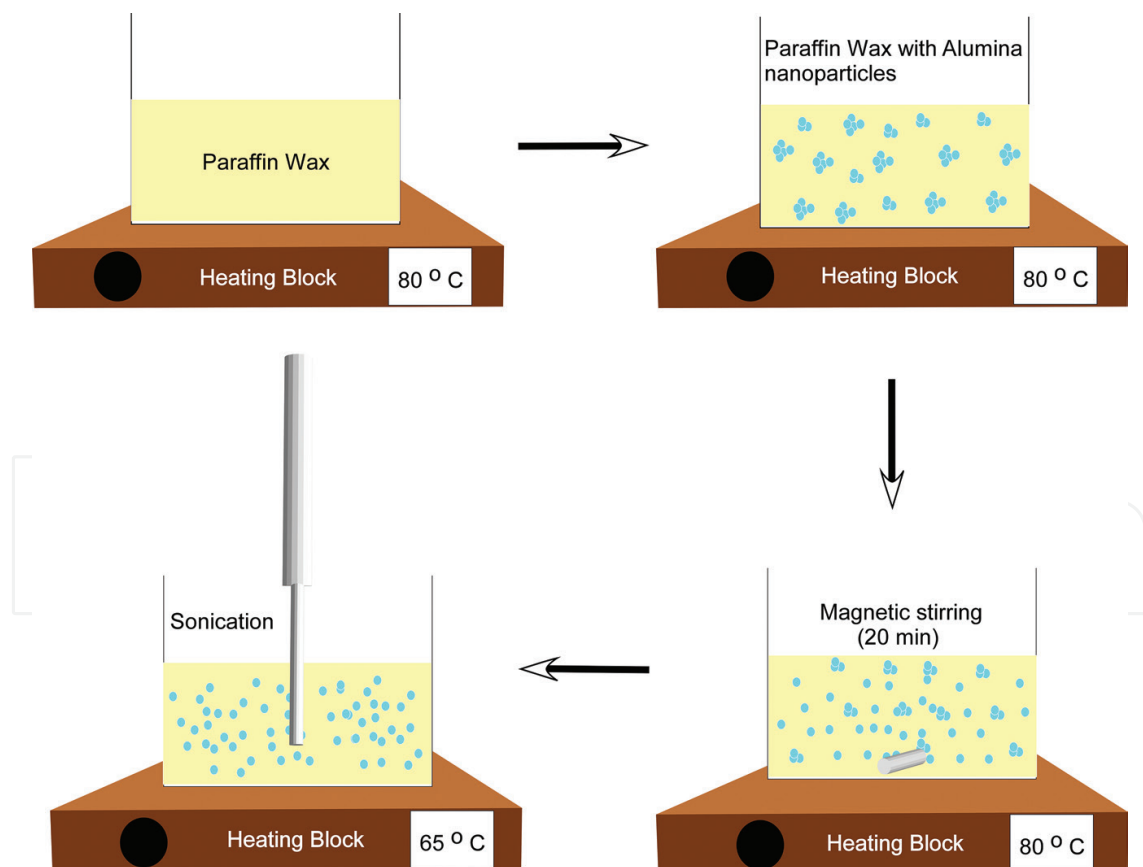

Figure 1. Preparation procedure of latent heat storage nanocomposite made of paraffin wax and alumina.

3. Thermal stability of nanocomposite PCMs

3.1. Differential scanning calorimetry

The phase change behavior of paraffin and paraffin/alumina composite involves two parameters: the latent heat and the phase change temperature, which can be measured by DSC (NETZSCH DSC 204) analysis. DSC thermogram of the paraffin and paraffin/alumina composite with 5 and 10 vol% of alumina nanoparticle is shown in **Figure 2a**, **b**, and **c**. The test results infer that nanocomposite exhibited only a single peak confirming to the solid-liquid transition, and no traces of solid-solid secondary peak were observed. These aspects are especially good for PCMs to maximize their heat storage and release capabilities at one stretch during melting and freezing cycles [11]. In DSC, the main peak represents the phase-change behavior of paraffin and paraffin/alumina composite. Phase change temperature is taken as onset temperature in DSC curve. With an increase in the volume fraction of alumina nanoparticle, the phase change temperature of paraffin/alumina composite increases and latent heat capacity of paraffin/alumina composite reduces compared to paraffin wax (heating curve) as shown in **Figure 2b** and **c**. The DSC results of paraffin, 5 vol%, and 10 vol% of alumina nanoparticle are presented in **Table 2**.

The melting temperature of 10 vol% of alumina shifted to 58.6°C, whereas paraffin was 58.9°C. On the other hand, the freezing temperature of 10 vol% of alumina shifted to 47°C, whereas paraffin wax was 44.4°C. The latent solid-liquid phase change for the composites are around 121 J/g, which is very close to the value of 124.4 J/g for pure paraffin. This is because no chemical reaction takes place between paraffin and nanoparticles in the preparation of nanocomposites. This is consistent with observations made by Ho and Gao [12] and Kim and Drzal [13]. Nanoparticle dispersions neither agree to affect the melting/freezing behavior nor the phase change temperature. The measured and calculated latent heat of paraffin/alumina composite is shown in **Table 3**. Using a simple mixture theory, the latent heat of fusion of the composite PCMs is calculated by:

$$\Delta H_{eff} = \Delta H_m \left(1 - \phi_v\right) \tag{1}$$

where ΔH_{eff} and ΔH_m stand for the calculated effective latent heat of fusion of composite PCMs and the measured latent heat of the fusion of the pure paraffin is 124.4 J/g (obtained by DSC at a scan rate of 1°C/min), respectively, and ϕ_v is the equivalent volume fraction of alumina. From **Table 3**, it is observed that latent heat of composite decreases with increase in volume fraction of alumina nanoparticle.

3.2. Comparison of DSC thermograms based on latent heat of nanoparticle embedded PCM with present study

3.2.1. Comparison of latent heat of Al$_2$O$_3$ nanoparticles in n-octadecane emulsion with present study
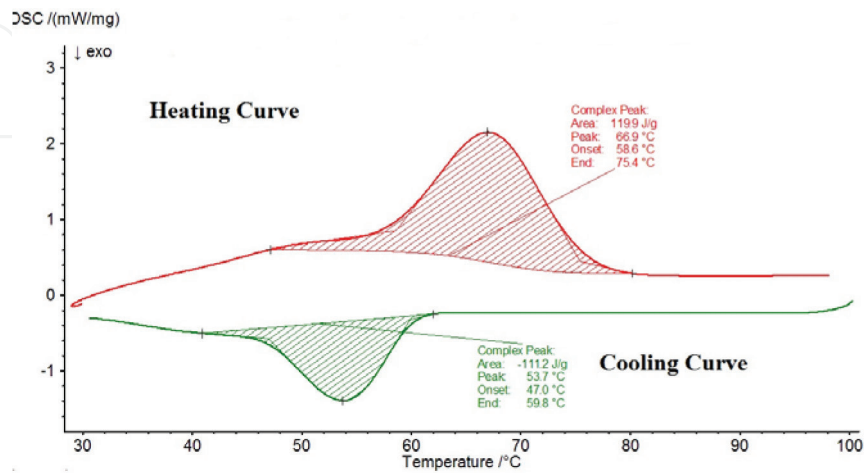
DSC thermograms of pure paraffin ($C_{18}H_{38}$) and Al$_2$O$_3$ nanoparticles in paraffin emulsion in various mass fractions 5 and 10 wt% are shown in **Figure 3**. The latent heat and phase change temperature are significantly different for paraffin-alumina emulsion composites.
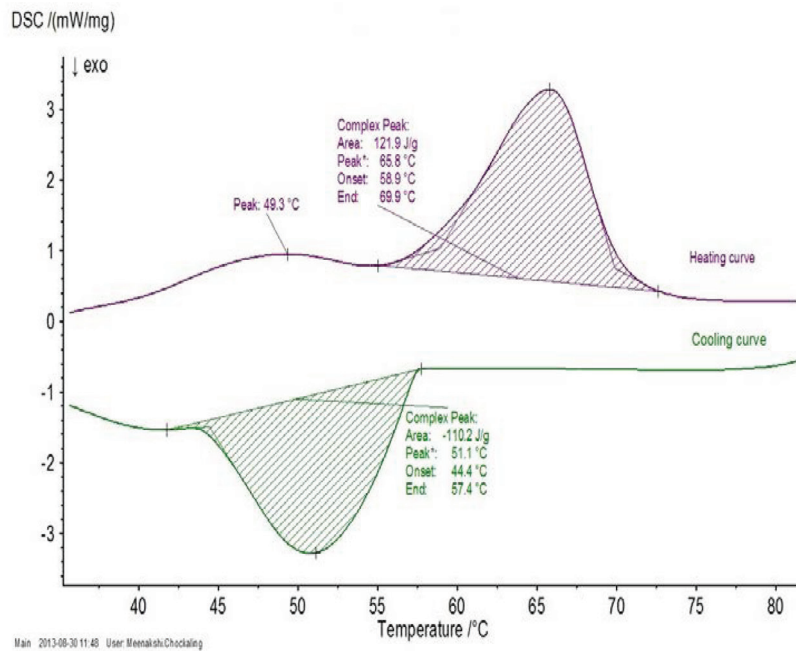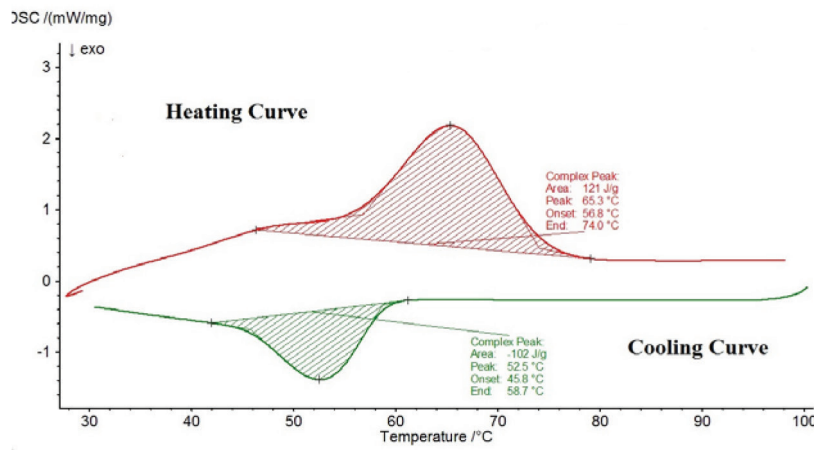
Figure 2. (a) DSC thermogram of paraffin wax, (b) DSC thermogram of composite with 5 vol% of alumina nanoparticle, and (c) DSC thermogram of composite with 10 vol% of alumina nanoparticle.

PCM/Composite	Melting temperature, T_m (°C)	Freezing temperature, T_f (°C)	Latent heat of fusion on heating curve (J/g)	Latent heat of fusion on cooling curve (J/g)
0 (paraffin wax)	58.9	44.4	121.9	−110.2
5 vol%	56.8	45.8	121	−102
10 vol%	58.6	47	119.9	−111.2

Table 2. Melting/freezing temperatures and latent heat of fusion of paraffin and composite.

Volume fraction of alumina, ϕ (%)	Phase change latent heat	
	Calculated value (J/g)	Experimental value (J/g)
5	122.85	121
10	121.90	119.9

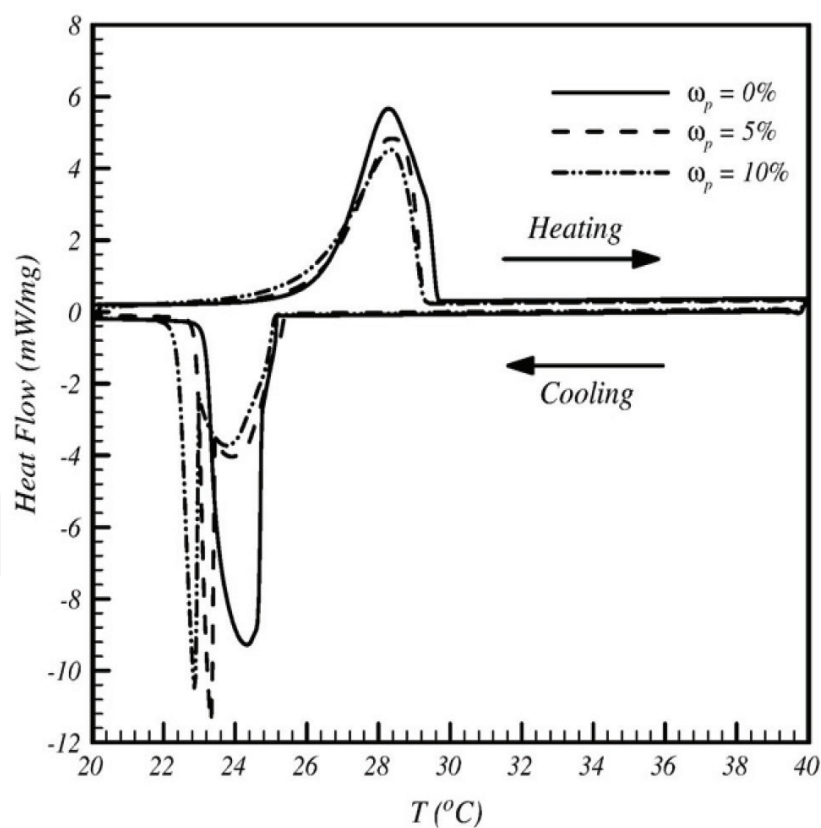Table 3. Experimental and calculated values of latent heat of fusion.

Figure 3. DSC thermograms of heating and cooling curves for Al_2O_3 in paraffin emulsions and pure paraffin ($C_{18}H_{38}$) in the range of 20–40°C [12].

Table 4 compares the latent heat of fusion of alumina nanoparticles in the *n*-octadecane emulsion with paraffin/alumina composites (scan rate @ 1°C/min). Latent heat of alumina-in-octadecane emulsion ($H_{Solid-liquid}$ = 212.3 kJ/kg) decreases with the increase in the mass fraction of alumina nanoparticles compared with that of the pure paraffin ($H_{Solid-liquid}$ = 243.1 kJ/kg), and the same trend is observed in our present study (**Table 2**). The measured values of the latent heat capacity of composites with 5 and 10 wt% are lower than that of pure paraffin ($C_{18}H_{38}$) by 7 and 13%, whereas the present study of latent heat of fusion of paraffin/alumina nanocomposites is nearly 8 and 14% for paraffin containing 5 and 10 vol% of alumina nanoparticles.

3.2.2. Comparison of latent heat of 10 wt% CNEP with present study

Figure 4 shows the DSC heating and cooling curve of 10 wt% copper oxide nanoparticle-enhanced paraffin (CNEP). The heating and cooling curve indicate two phase transition peaks.

Nanoparticle mass fraction (W_p)	Latent heat of fusion on heating curve (kJ/kg)	Nanoparticle volume fraction (ϕ)	Latent heat of fusion on heating curve (J/g)
0	243.1	0	124.4
5 wt%	225.6	5 vol%	114.3
10 wt%	212.3	10 vol%	107.2

Table 4. Comparison of latent heat of fusion of Al_2O_3—in octadecane emulsion with present study.
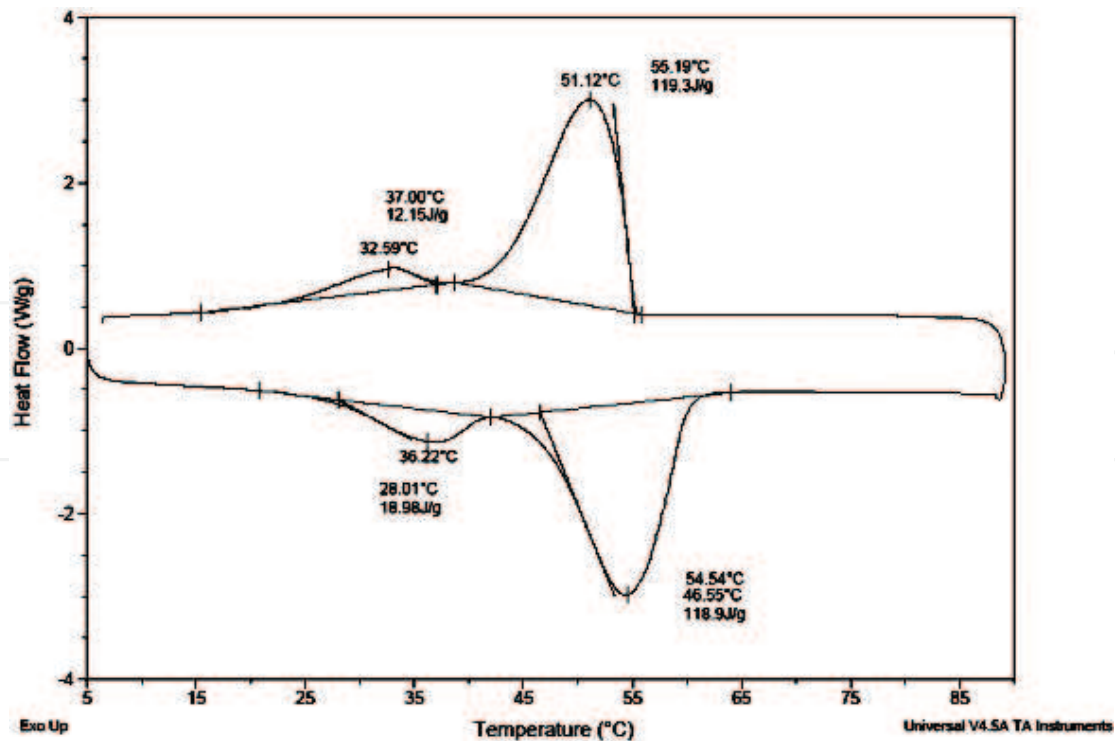

Figure 4. DSC thermograms of 10 wt% copper oxide nanoparticle enhanced paraffin [5].

The primary peak at around 35°C corresponds to the solid-solid phase change in paraffin, and the secondary peak at around 55°C corresponds to the solid-liquid phase change. The latent heat solid-liquid of 10 wt% copper oxide nanoparticle-enhanced paraffin is 119.3 J/g, which is very close to the value of 119.9 J/g for 10 vol% of alumina nanoparticle-enhanced paraffin.

4. Thermophysical properties of nanocomposite PCMs

4.1. Specific heat capacity

The specific heat is one of the important properties and plays an important role in influencing heat transfer rate in nanocomposite. Predicted specific heat values (C_p) of the nanocomposite for various volume fraction can be calculated using mixture formula Eq. (2), and it is shown in **Table 5**. This formula is valid for homogenous mixtures.

$$C_{p\,nanocomposite} = \frac{(1-\phi)(\rho C_p)_{bf} + \phi(\rho C_p)_{np}}{\rho_{ANEP}} \qquad (2)$$

As the thermal conductivity of nanocomposites is expected to be higher due to high thermal conductivity of Al_2O_3 particles, the nanocomposites show higher ability to conduct heat. This obviously results in lower heat storage capacity. From **Table 5**, it is depicted that the specific heat of nanocomposites decreases, the volume fraction of nanoparticle will be increased.

4.2. Improvement in thermal conductivity of nanocomposite

4.2.1. Thermal conductivity measurement

Thermal conductivity is measured by the procedure given in the literature [14]. However, a constant temperature hot water bath was also incorporated to maintain the composite at constant temperature to avoid solidification of the samples during the measurement. Thermal conductivity measurement of nanocomposite was made by KD2 Pro thermal property analyzer (Decagon Devices, Inc.; USA). Schematic view of KD2 Pro thermal property analyzer is shown in **Figure 5**. The KD2 Pro analyzer consists of a handheld microcontroller along with sensor needles. The sensor needle is composed of a heating element and thermistor. The controller module consists of three sets of batteries, a 16 bit microcontroller/AD converter, and power control circuit. The sensor needle (KS-1) made of stainless steel is 60 mm long and has a diameter of 1.3 mm and closely approximates an infinite line heat source. Each measurement cycle lasts for 90 s and consists of three stages. The instrument will equilibrate during the first

Volume fraction (ϕ) (vol%)	Specific heat capacity of nanocomposite (J/kg K)
5	2793
10	2686

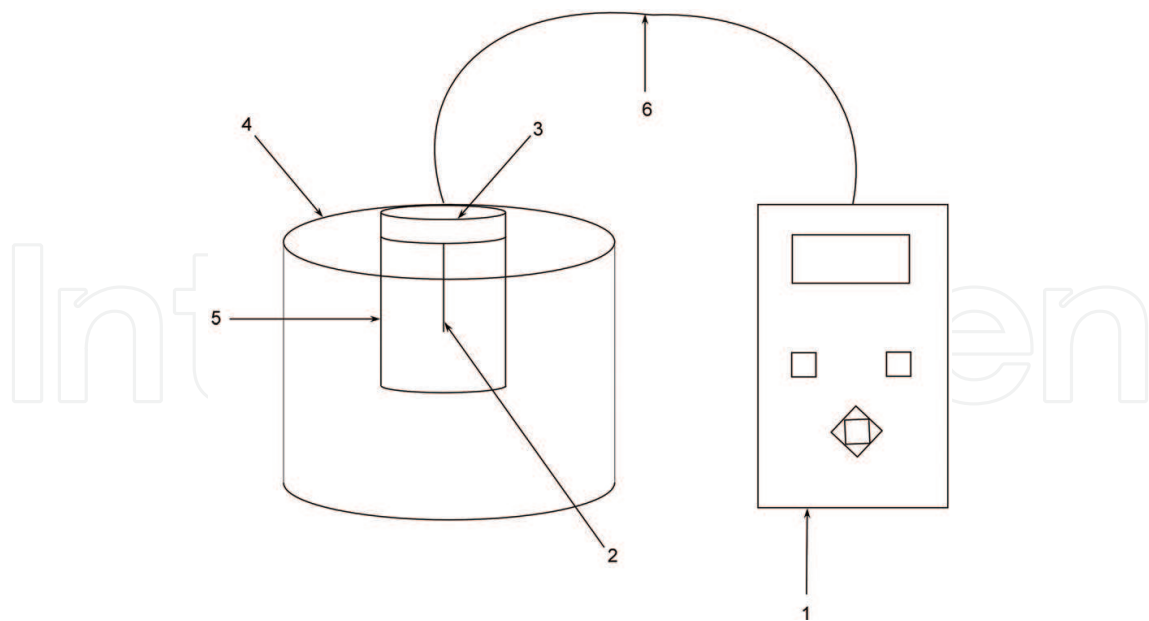**Table 5.** Specific heat capacity of nanocomposite.

Figure 5. Schematic sketch of KD2 pro thermal property analyzer. 1-Microcontroller, 2-Sensor, 3-Septum, 4-Hot water bath, 5-Vial, 6-Cable.

30 seconds, which is followed by heating and cooling of the sensor needles for 30 seconds each. At the end of the reading, the controller computes the thermal conductivity using the change in temperature (ΔT)-time data as per Eq. (3).

$$k = \frac{q(\ln T_2 - \ln T_1)}{4\pi(\Delta T_2 - \Delta T_1)} \tag{3}$$

where q is the constant heat rate applied to an infinitely long and small "line" source, ΔT_1 and ΔT_2 are the changes in the temperature at times t_1 and t_2, respectively.

Thermal conductivity is the most important property of phase change materials and need detailed investigation. The thermal conductivity was measured as a function of temperature with respect to nanoparticle loading. **Figure 6** depicts the thermal conductivities of paraffin and composite assessed at various temperatures. It is explicit from the **Figure 6** that the influence of temperature on the thermal conductivity of paraffin as well as composites is less significant in solid and liquid states.

However, an atypical rise in thermal conductivity was observed near the solid - liquid phase change temperature, and the same suddenly falls down when the paraffin wax and nanocomposite PCM turned completely into liquid state. Thermal conductivity of paraffin wax and composites of various volume concentration is summarized in **Table 6**. The increase in thermal conductivity near the phase change is attributed to the accelerated molecular vibrations in the matrix of ordered solid structure when the temperature was increased [15]. The thermal conductivity of the composite with 5 vol% of alumina is 0.2677 W/mK at 45°C in the solid state and 0.24 W/mK at 65°C in the liquid state. After phase change, there is a breakage of the orderly solid structure into a disorderly liquid structure, and therefore, the thermal conductivity of
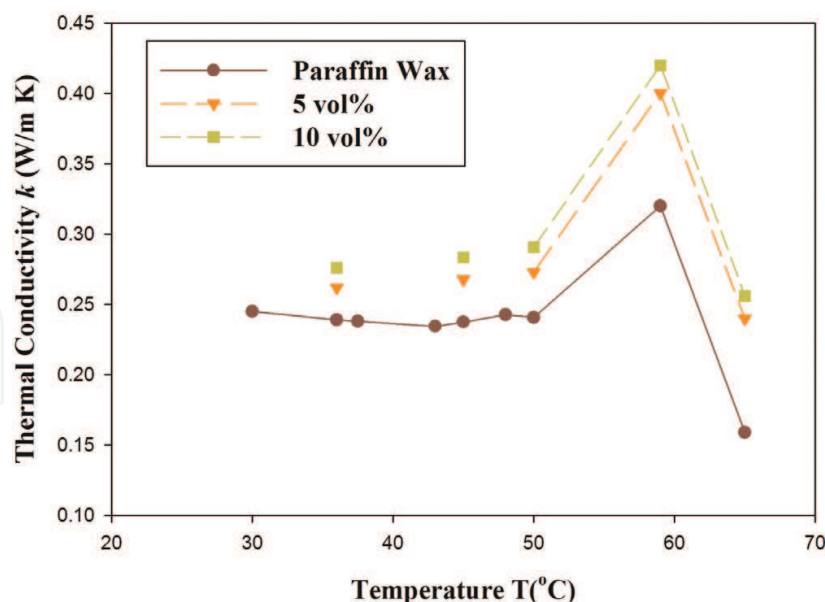
Figure 6. Thermal conductivity of paraffin wax and composite versus temperature.

paraffin wax and composite has become less than that in the solid state. The thermal conductivity of the paraffin wax is 0.2375 W/mK (45°C) in solid state and 0.1590 W/mK (65°C) in the liquid state. Thermal conductivity of composite with 10 vol% of alumina is higher than paraffin wax by 0.2834 W/mK at 45°C and 0.2560 W/mK at 65°C. However, higher thermal conductivity measured, i.e., k = 0.42 W/mK for 10 vol% of alumina at 59°C (close to the phase change temperature), is desirable for LHTES applications.

Thermal conductivity enhancement ratio was calculated by $\Psi = (k_c - k_p)/k_p$ with k_c being the thermal conductivity of composite and k_p thermal conductivity of paraffin wax, respectively. The thermal conductivity ratio of composites assessed at different temperatures for various volume concentration is depicted in **Figure 7**. The thermal conductivity enhancement of

Temperature (°C)	Thermal Conductivity (W/mK)		
	Paraffin wax	ϕ = 5 vol%	ϕ = 10 vol%
30	0.2450		
36	0.2390	0.2620	0.2760
37.5	0.2380		
43	0.2344		
45	**0.2375**	**0.2677**	**0.2834**
48	0.2427		
50	0.2406	0.2729	0.2906
59	0.3200	0.4000	0.4200
65	**0.1590**	**0.2400**	**0.2560**

Note: Show the temperature values in solid and liquid state (Bold).

Table 6. Thermal conductivity of paraffin and various volume fraction of alumina at different temperature.
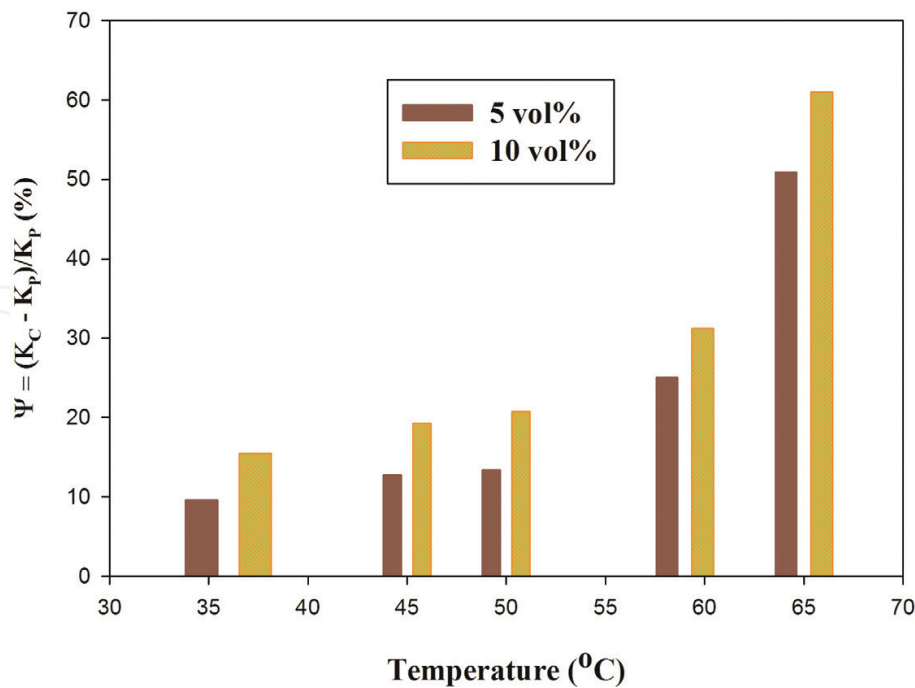
Figure 7. Thermal conductivity of composite as a function of temperature.

composite (5 vol% of alumina) is 12.71% at 45°C in solid state and 50.94% at 65°C in liquid state. For example, in 10 vol% of alumina, the enhancement ratio of composite is 19.32% at 45°C and 61% at 65°C in solid and liquid state, respectively. The thermal conductivity of the composite increased with an increase in the volume fraction of Al_2O_3, and also, the enhancement in liquid state (at 65°C) was higher than that in the solid state. The higher enhancement of the composite is attributed to more alumina addition. However, in the present study, the enhancement ratio of paraffin/alumina composite has improved from 9.62 to 61% for 5 and 10 vol% of alumina, respectively. Thermal conductivity of alumina is ($k = 36$ W/mK); the composites are expected to have considerable higher thermal conductivity than that of the paraffin wax. The higher enhancement in liquid state was primarily due to the enhanced Brownian motion of nanoparticles within the base fluid having considerably reduced viscosity due to increase in temperature, and it is discussed in detail in Section 4.5.1. Enhancement of thermal conductivity is due to deposition of nanoparticles in melting interface and agglomeration of the nanoparticle.

The liquid molecule close to particle surfaces is known to form layered structures and behave much like a solid. The results also showed that the thermal conductivity of paraffin could be achieved further by the addition of alumina more than 10 vol% of alumina nanoparticle. However, this volume fraction is adequate to obtain form-stable composite PCM, and further increase in alumina over 10 vol% of alumina nanoparticle will result in an increase in a latent heat capacity of the composite.

4.2.2. Comparison of thermal conductivity with Maxwell model

The theoretical thermal conductivity of solid phase paraffin/alumina composite PCMs was calculated using Maxwell's model [16].

$$k_{pred} = k_{bf} \times \frac{k_p + 2k_{bf} - 2\phi_v (k_{bf} - k_p)}{k_p + 2k_{bf} + \phi_v (k_{bf} - k_p)} \qquad (4)$$

where k_p is the thermal conductivity of the dispersed nanoparticles, thermal conductivity of alumina nanoparticle (k_p) is 36 W/mK, k_{bf} is the thermal conductivity of the base fluid in liquid medium, and ϕ_v is the equivalent volume fraction of the nanoparticles.

Table 7 shows the measured and predicted thermal conductivity of various ANEP samples at 45°C, and it is compared with Arasu [9] predicted Maxwell model at 47°C. Enhancement of thermal conductivity measurement is slightly higher than the theoretical predicted result. This is attributed to the fact that the interaction between the high-conductive alumina nanoparticles and the matrix molecule affecting the relative thermal conductivity of NEPCMs [17]. The predicted thermal conductivity values of Arasu (@ 47°C) were 1ower than our recent study.

4.3. Comparison of thermal conductivity enhancement of various nanocomposite-based PCMs with present study

4.3.1. Thermal conductivity enhancement of Al$_2$O$_3$ nanoparticle-in-octadecane emulsion

Table 8 compares the increase in thermal conductivity of pure paraffin($C_{18}H_{38}$)-nanoparticle composites of various phases with the present study. Relative thermal conductivity enhancement of more than 2 and 6% for the paraffin containing 5 and 10 wt% of alumina nanoparticle at temperature 30°C. The enhancement of thermal conductivity in a liquid state of Al$_2$O$_3$ nanoparticle in n-octadecane (W_p = 10 wt%) was found to be more than 17% as the temperature is increased up to 60°C. Thermal conductivity enhancement of Ho and Gao [12] was lower than our present study (**Table 8**). Ho and Gao used n-octadecane with the melting point of 25.1–26.5°C, whereas in the recent study, paraffin wax was used as a phase change material with a melting point of 58–60°C.

Volume fraction (ϕ)	k_{meas} (W/mK)	k_{pred} (W/mK)	Predicted Maxwell model with Arasu (W/mK)
0	0.2375	0.2375	0.12
5 vol%	0.2677	0.2462	0.17
10 vol%	0.2834	0.2559	0.22

Table 7. Measured and calculated ANEP samples at 45°C (solid state).

State	Temperature (°C)	10 vol% ANEP	Temperature (°C)	10 wt%(n-octadecane-alumina emulsion)
Solid	45	19.32%	30	6%
Liquid	65	61%	60	17%

Table 8. Percentage increase in thermal conductivity during solid and liquid phases.

4.3.2. Comparison of thermal conductivity enhancement of 10 wt% CuO nanoparticle enhanced paraffin of different phases with present study (10 vol% of ANEP)

Figure 8 compares the percentage increase in thermal conductivity of 10 wt% CNEP with the present study. Enhancement in thermal conductivity in the liquid state was more pronounced than in the solid state or during phase change.

A maximum of 61% (0.2560 W/mK for ANEP as compared to 0.1590 W/mK for pure paraffin) and 16.35% (0.185 W/mK for CNEP as compared to 0.1590 W/mK for pure paraffin) enhancement of thermal conductivity in the liquid state at 65°C have been achieved in 10 vol% ANEP and 10 wt% CNEP respectively. A maximum of 31.25% (0.42 W/mK for ANEP as compared to 0.32 W/mK for pure paraffin) and 14.37% (0.35 W/mK for CNEP as compared to 0.3060 W/mK for pure paraffin) enhancement of thermal conductivity during phase change (59°C) was achieved in 10 vol% ANEP and 10 wt% CNEP, respectively. A maximum of 19.32% (0.2834 W/mK for ANEP as compared to 0.2375 W/mK for pure paraffin) and 13.04% (0.26 W/mK for CNEP as compared to 0.23 W/mK for pure paraffin) enhancement of thermal conductivity in the solid state at 45°C was found in 10 vol% ANEP and 10 wt% CNEP, respectively. It can be clearly seen that aluminum oxide nanoparticles lead to a higher thermal conductivity enhancement than copper oxide nanoparticles, even though the size of the copper nanoparticles was less than that of the alumina nanoparticles.

4.4. Density of the nanocomposite PCMs

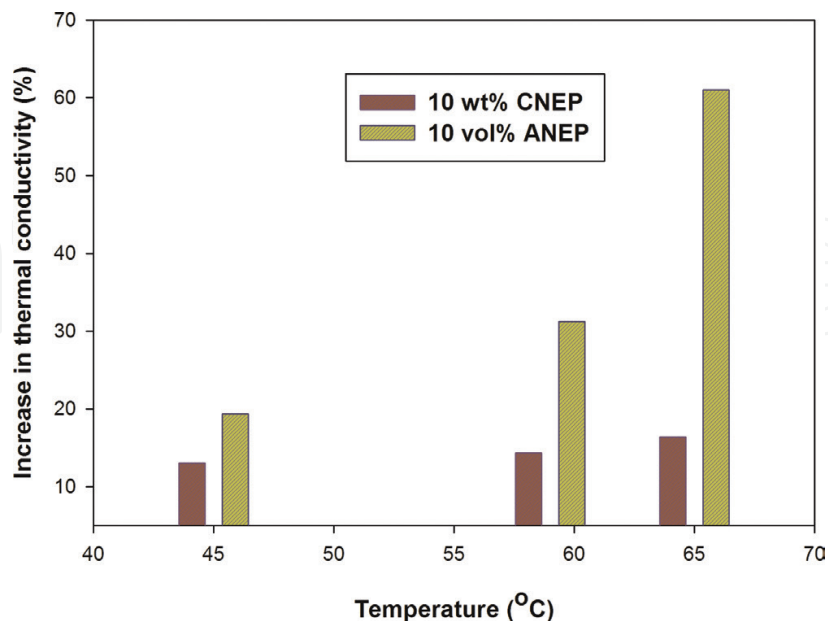The density of nanocomposite is determined using density-correlation equation developed by Pak and Cho [18].

Figure 8. Comparison of percentage increase in thermal conductivity during different phases.

$$\rho_{Nanocomposite} = \varphi\rho_{np} + (1-\varphi)\rho_{bf} \tag{5}$$

where

ρ_{np}—Density of Al$_2$O$_3$ nanoparticle, kg/m^3.

ϕ_v—Equivalent volume concentration of alumina nanoparticle.

ρ_{bf}—Density of the base fluid, kg/m^3.

The density of the nanocomposites is calculated using the correlation and is presented in **Table 9**.

Since the density of Al$_2$O$_3$ particles is much higher than paraffin wax, the quantity of nano particles replacing equivalent volume of paraffin wax in the composite would add more mass. Hence, the density of nanocomposites increases with increase in volume fraction of nano particles.

4.5. Viscosity measurement

The viscosity of the composite was measured by using Brookfield cone and plate viscometer (LVDV-I PRIME C/P) equipped with a 2.4 cm 0.8°cone supplied by Brookfield Engineering Laboratories, USA, is shown in **Figure 9**. In Brookfield cone and plate viscometer, the cone is connected to the spindle drive, whereas the plate is mounted in the sample cup. Water at a constant temperature of 60°C, 65°C, and 70°C was circulated to the outer surface of the sample cup from a constant temperature hot water bath to prevent the solidification of the samples in the cup, maintain the temperature constant, and measure the viscosity. Measurements were done at three different temperatures for each sample. To measure viscosity in the range of 0.3–1028 cP, spindle CPE-40 was used. Between the plate and cone, a gap of 0.013 is maintained. An adjusting feature of the cone and plate Viscometer is an electronic gap, which is used to place the test fluid in the gap. To rotate the spindle, the viscous drag of the fluid is measured by spring deflection. To attain the temperature equilibrium quickly within a minute, the sample volume required is 0.5–2 ml. To obtain adequate results in spindle/speed combination when applied torque is between 10 and 100% of maximum permissible torque. Measurement can be taken as superfluous if the applied torque does not fall within the possible range. Readings were discarded if the applied torque did not fall within this prescribed range. In cone and plate viscometer, the spindle speed is in the range of 0–100 rpm, and the shear rate is 0–750 s^{-1}.

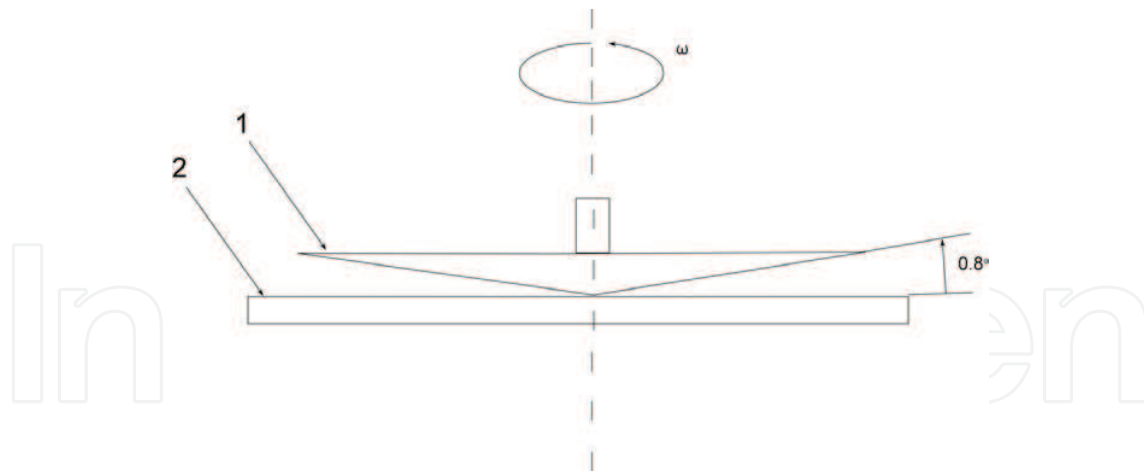| Volume fraction (ϕ) (vol%)	Equivalent volume fraction (ϕ_v)	Density of nanocomposite (kg/m^3)
5	0.0124	893.976
10	0.0258	930.692

Table 9. Density of nanocomposite.

Figure 9. Cone and plate assembly. 1. Cone; 2. Plate.

4.5.1. Experimental measurement on dynamic viscosity

Figure 10 shows the measured dynamic viscosity of paraffin and volume fraction of alumina at various temperatures, respectively. The dynamic viscosity decreases with temperature and increases with an increasing volume fraction of alumina nanoparticles is shown in **Figure 10**. This shows that the addition of nanoparticles makes paraffin more viscous. **Table 10** presents the dynamic viscosity of paraffin and various volume fractions of alumina at different temperatures, respectively. **Figure 10** indicates that the dynamic viscosity has a nonlinear increase with nanoparticle concentration for paraffin-nanoparticle composites. In the liquid state, dynamic viscosity decreases sharply with temperature, while the thermal conductivity has a weak dependence on temperature. For a particular concentration of nanoparticles,
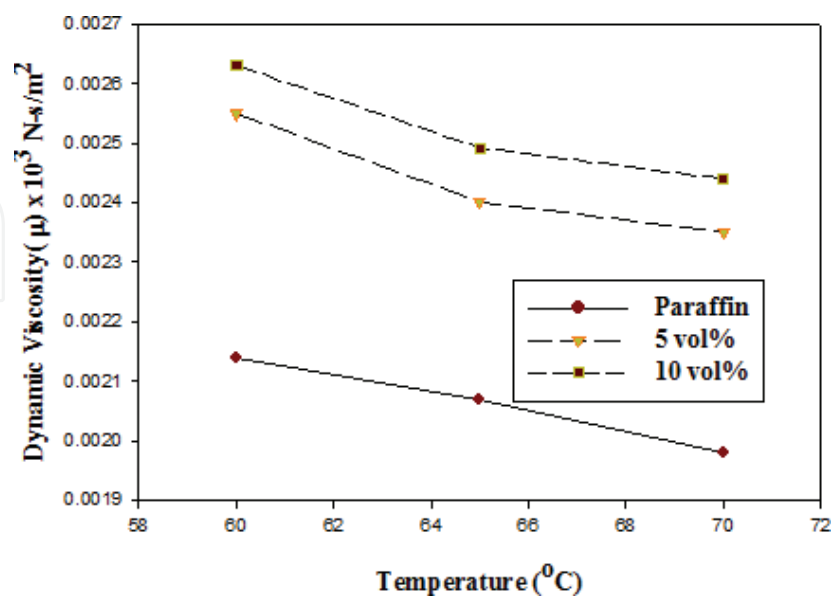

Figure 10. Measured dynamic viscosity for various volume fraction of alumina from 60 to 70°C.

Temperature (°C)	Dynamic viscosity (Cp)		
	Paraffin wax	5 vol%	10 vol%
60	2.14	2.55	2.63
65	2.07	2.401	2.492
70	1.98	2.35	2.44

Table 10. Dynamic viscosity of paraffin and various volume fractions of alumina at different temperature.

Volume fraction (ϕ) (vol%)	Dynamic viscosity of nanocomposite (Ns/m²)
5	0.2114
10	0.2188

Table 11. Dynamic viscosity of nanocomposite.

the increase in dynamic viscosity is almost the same at different temperatures, while the enhancement of thermal conductivity increases with increase in temperature. So, at higher temperatures, the thermal conductivity enhancement will shoot over the percentage increase in dynamic viscosity.

4.5.2. Comparison of viscosity with Brinkman's correlation

The viscosity of the ANEP samples is predicted using the Brinkman's correlation [19] and is given by:

$$\mu_{Pred} = \mu_{bf} \times \frac{1}{(1 - \phi_v)^{2.5}} \tag{6}$$

where μ_{Pred} is predicted viscosity, μ_{bf} is viscosity of the base fluid, and ϕ_v is the eqivalent volume fraction of particles in base fluid. The dynamic viscosity of the composites is shown in **Table 11**. From **Table 11**, it is depicted that dynamic viscosity increases with increase in volume concentration of the nanoparticle.

5. Conclusion(s)

1. Nanoparticle enhanced paraffin composites were then prepared by dispersing the aluminum oxide nanoparticles in liquid paraffin under the intense signification to make the mixture stable.

2. The effect of nanoparticle volume concentration and the temperature was also investigated. Differential scanning calorimetry reveals that there is only one peak during meting/freezing cycle in paraffin/alumina composites and latent heat decreased with the addition of alumina nanoparticles compared to paraffin wax. There is no significant difference in latent heat value between the 10 vol% ANEP and 10 wt% CNEP.

3. Relative thermal conductivity enhancement of Ho and Gao (17%) was lower than our present study. Compared to Ho and Gao, the latent heat of paraffin/alumina composites was nearly 8 and 14%.

4. It was found that increase in thermal conductivity of ANEP is consistently higher than that of CNEP. The maximum increase in thermal conductivity (61%) was observed for 10 vol% ANEP in the liquid state at 65°C. The maximum increase in dynamic viscosity (23%) was observed for 10 vol% ANEP at 70°C.

5. Maxwell's model of the predicted result (k = 0.22 W/mK @ 47°) in Arasu was higher than that of recent studies (k = 0.2559 W/mK @ 45°)

6. Final suggestion

This chapter is presented to be only a baseline study to study the charging and discharging characteristics of horizontal double pipe latent heat energy storage system. This is a very important topic and will be addressed in later chapter.

Nomenclature

A	external surface area of heat transfer fluid pipe (m²)
C_p	specific heat of PCM/alumina (kJ/kg°C)
H	latent heat of paraffin/composite (J/g or kJ/kg)
M	mass of PCM (kg)
T	temperature (°C)
t	time (min)

Greek symbols

μ	dynamic viscosity of paraffin wax(kg/m s)
ρ	density (kg/m³)
W	weight
ϕ	volume fraction
Ψ	thermal conductivity enhancement ratio

Subscripts

eff	effective
bf	base fluid
m	melting temperature/composite

v	volume fraction or volume
l	liquid
s	solid
w	water
f	freezing temperature
c	nanocomposite
p	paraffin wax/copper oxide nanoparticle/alumina nanoparticle
k	thermal conductivity (W/m K)

Abbreviations

DSC	differential scanning calorimetry
LHTESS	latent heat thermal energy storage system
ANEP	alumina nanoparticle enhanced paraffin
CNEP	copper-oxide nanoparticle enhanced paraffin
PCM	phase change material

Author details

Ponnuraj Stella Jesumathy

Address all correspondence to: jesumathy81@gmail.com

Independent Scientist, Erode, India

References

[1] Francis A, Neil H, Philip E. A review of materials, heat transfer and phase change problem formulation for latent heat thermal energy storage systems (LHTESS). Renewable Sustainable Energy Review. 2010;**14**:615-628

[2] Atul S, Tyagi VV, Chen CR. Review on thermal energy storage with phase change materials and applications. Renewable Sustainable Energy Review. 2009;**13**:318-345

[3] Zalba B, Martin JM, Cabeza LF, Mehling H. Review on thermal energy storage with phase change: Materials, heat transfer analysis and applications. Applied Thermal Engineering. 2003;**23**:251-283

[4] Shukla A, Buddhi D, Sawhney RL. Solar water heaters with phase change material thermal energy storage medium. Renewable Sustainable Energy Review. 2009;**13**(8):2119-2125

[5] Jesumathy S, Udayakumar M, Suresh S. Experimental study of enhanced heat transfer by addition of CuO nanoparticle. Heat and Mass Transfer. 2012;**48**:965-978

[6] Elgafy A, Lafdi K. Effect of carbon nanofiber additives on thermal behavior of phase change materials. Carbon. 2005;**43**(15):3067-3074

[7] Jegadheeswaran PSD. Performance enhancement of latent heat thermal storage system: A review. Renewable and Sustainable Energy Reviews. 2009;**13**:2225-2244

[8] Zeng JL, Zhu FR, Yu SB, Zhu L, Cao Z, Sun LX, Deng GR, Yan WP, Zhang L. Effects of copper nanowires on the properties of an organic phase change material. Solar Energy Materials and Solar Cells. 2012;**105**:174-178

[9] Arasu AV, Agus Sasmito P, Arun MS. Numerical study of paraffin wax dispersed with alumina in a concentric pipe latent heat storage system. Thermal Science. 2013;**17**(2):419-430

[10] Arasu AV, Agus Sasmito P, Arun Mujumdar S. Numerical evaluation of laminar heat transfer enhancement in nanofluid flow in coiled square tubes. Nanoscale Research Letters. 2011;**6**(1):376

[11] Aydin AA, Okutan H. High chain fatty acid esters of myristyl alcohol with odd carbon number: Novel organic phase change materials for thermal energy storage-2. Solar Energy Materials and Solar Cells. 2011;**95**:2417-2423

[12] Ho CJ, Gao JY. Preparation and thermophysical properties of nanoparticles in paraffin emulsions phase change material. International Communications in Heat and Mass Transfer. 2009;**36**:467-470

[13] Kim S, Drzal LT. High latent heat storage and high thermal conductive phase change materials using exfoliated graphite nanoplatelets. Solar Energy Material and Solar Cells. 2009;**93**:136-142

[14] Chandrasekar M, Suresh S, Chandra Bose A. Experimental investigation and theoretical determination of thermal conductivity and viscosity of Al_2O_3/water nanofluid. Experimental Thermal and Fluid Science. 2010;**34**:210-216

[15] Wang J, Xie H, Xin Z, Li Y, Chen L. Enhancing thermal conductivity of palmitic acid based phase change materials with carbon nanotubes as fillers. Solar Energy. 2010;**84**:339-344

[16] Hashin Z, Shtrikman S. A variational approach to the theory of the effective magnetic permeability of multiphase materials. Journal of Applied Physics. 1962;**33**:3125-3131

[17] Xue Q. Model for effective thermal conductivity of nanofluids. Physics Letters. 2003; **307**:313-317

[18] Pak BC, Cho YI. Hydrodynamic and heat transfer study of dispersed fluids with submicron metallic oxide particles. Experimental Heat Transfer. 1998;**11**:151-170

[19] Brinkman HC. The viscosity of concentrated suspensions and solutions. Chemical Physics. 1952;**20**:571